

Roles of intrinsically disordered regions in transcription factor search

Wencheng Ji,^{1,2} Ori Hachmo,¹ Naama Barkai,³ and Ariel Amir^{1,2}

¹*Department of Physics of Complex Systems, Weizmann Institute of Science, 234 Hertzl St., Rehovot, Israel*

²*John A. Paulson School of Engineering and Applied Sciences,
Harvard University, Cambridge, MA 02138, USA*

³*Department of Molecular Genetics, Weizmann Institute of Science, Rehovot, Israel*

Transcription Factors (TFs) are proteins that regulate gene expression. The regulation mechanism is via the binding of a TF to a specific part of the gene associated with it, the TF’s target. For the regulation to be effective, the TF has to be able to bind to the correct target and it should do so fast enough to allow the cell an appropriate reaction time to, e.g., the discovery or food or the detection of toxins. At the same time, the search process is limited to diffusive (slow) motion and to an environment saturated with “false” targets, other parts of the DNA with similar sequences. In eukaryotic cells many TFs have an Intrinsically Disordered Region (IDR) – a long polymeric “tail” constructed of hundreds of amino acids. The IDR of certain TFs were shown to take a key part in the search process and in this letter we develop a model that attempts to explain its contribution. We show that the IDR enables high affinity of the TF for its corresponding target and that the manner in which it does so could also shorten the search time.

Transcription Factors (TFs) are proteins designated to regulate gene expression in cells. The regulation mechanism is via the binding of a TF to the regulatory DNA regions associated with the genes, the TF’s target. For the regulation to be an effective mechanism, TFs are required to have sufficient binding affinity for their targets and a binding rate that is comparable with the processes taking place within the cell. In eukaryotic cells, besides having a DNA-binding domain (DBD), 80% of TFs also have one or more intrinsically disordered regions (IDRs), which lack a stable 3D structure and can therefore be thought of as unstructured polymers, hundreds of amino acids in length [1–4]. IDRs play a significant role in promoting target recognition [5–7], by increasing the interaction surfaces, thereby reducing the dimensionality of the search [8]. Recent *in vivo* experiments done in yeast suggest that IDRs could take a key part in guiding TFs to the DNA regions containing their targets [9].

There exists a vast collection of theoretical studies for the analogous problem. Most of those studies, however, consider parameters derived from bacterial studies. A prominent example is the facilitated diffusion mechanism – this mechanism was well-studied theoretically [10–15] and empirical evidence supporting it was found [16]. According to this model the TF performs 1D diffusion along the DNA and at any given moment can fall off and perform 3D diffusion until reattaching to the DNA (a 3D excursion). The 1D diffusion along the DNA and the 3D excursions happen interchangeably until the TF finds its target. However, due to the significant structural differences, including the larger genome size and chromatin structure, the facilitated diffusion mechanism is expected to be lacking in explaining the search mechanism in eukaryotes and a qualitatively different mechanism is required [17, 18].

In this letter we approach the problem of TF search in eukaryotes from two different angles – we discuss the

binding affinity quantified by the binding probability from an equilibrium point of view and then proceed to tackle the dynamic nature of the problem quantified by the search time. We obtain the optimality principles for both binding probability and search time, respectively, which result in significant improvements when compared to simple TFs that lack IDRs. The binding probability is shown to increase dramatically for TFs having IDRs (see Fig. 1(a)) for a broad parameter regime. The optimal search process consists of one round of 3D–1D search, where at first the TF performs 3D diffusion and then binds the DNA and performs 1D diffusion until finding its target, rarely unbinding for another 3D diffusion episode. This process is presented in Fig. 1(b,c). We obtain a semi-analytical expression for the search time that shows good agreement with our numerical results.

Binding affinity of the TF from the equilibrium approach— The experiment described in Ref. [9] studied the binding affinity of wild-type and mutated TFs to their corresponding targets. They found that shortening the IDR length results in weaker affinity. To qualitatively model the binding affinity of a TF to its target, we utilize a well-known physical model of polymers, the Rouse Model [19, 20]. The Rouse Model describes a polymer as a chain of point masses connected by springs and characterized by a statistical segment length l_0 resulting from the rigidity of springs k and the thermal noise level $k_B T$, $l_0^2 = 3k_B T/k$ [19, 20]. We model the segment of the DNA where targets reside as a straight line. The targets are positioned at equal spacing, with one target for the DBD and a few targets for the IDR. We coarse-grain the TF by representing it with a few binding sites for the IDR, and an additional site for the DBD. The setup for our calculations is shown in Fig. 1(a). In the Rouse Model, the 3D probability density describing the relative distance, denoted as r , between any two sites can be derived through

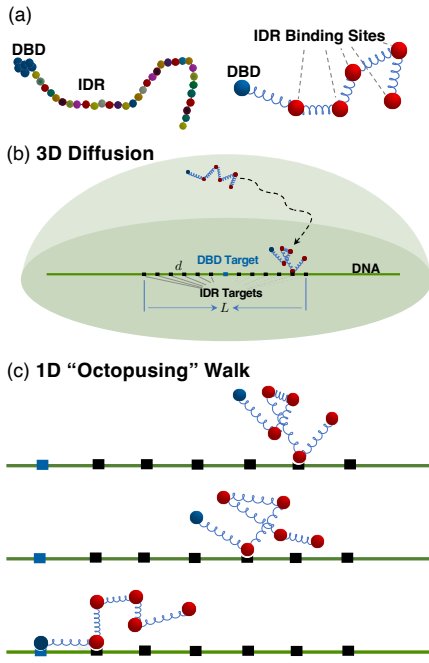


Figure 1. (a) Left: a sketch of a TF containing an IDR comprised of amino acids. Right: the TF model, a polymer chain connected by springs, comprises a single binding site for the DBD and multiple binding sites for the IDR. (b) The first stage of the search process: the TF performs 3D diffusion until it binds the DNA in a neighborhood of its target. (c) Once bound to the DNA, the TF performs effective 1D diffusion until reaching its target. The 1D diffusion is via the binding and unbinding of sites along the IDR, a process we name “octopusing”.

Gaussian integration [20], leading to:

$$f(r, l) = \left(\frac{3}{2\pi l^2} \right)^{\frac{3}{2}} \exp\left(-\frac{3r^2}{2l^2}\right), \quad (1)$$

where $l = \sqrt{n}l_0$ and n is the number of segments between the two sites. l is equal to $\sqrt{\int d^3r r^2 f(r, l)}$, indicating the typical distance of the two sites.

We then start by considering the simple case of a TF that has a single IDR site. We assume that the IDR has only one corresponding target. There are four possible states: neither the DBD nor the IDR are bound, the IDR is bound, the DBD is bound, and both are bound, which correspond to P_{free} , P_{IDR} , P_{DBD} , and P_{both} , respectively. Using equilibrium statistics, we have (see the derivation in S1 of the Supplemental Material (SM)):

$$P_{\text{IDR}}/P_{\text{free}} = \nu \exp(E_B), \quad (2a)$$

$$P_{\text{DBD}}/P_{\text{free}} = \nu \exp(E_{\text{DBD}}), \quad (2b)$$

$$P_{\text{both}}/P_{\text{free}} = \nu \exp(E_B + E_{\text{DBD}}) V_1 f(d, l_0), \quad (2c)$$

where ν is the ratio of the target volume to the nucleus volume, $-E_{\text{DBD}}$ ($-E_B$) is the binding energy for the DBD

(IDR) target, V_1 is the target volume, and d is the distance between the two targets, which is much larger than the target’s size. In our convention, E_{DBD} and E_B are positive, and $k_B T$ is set to 1. The probability that the TF is bound at the DBD target, the sum of P_{DBD} and P_{both} , thus reads

$$P_{\text{TF}} = \frac{r_{\text{DBD}} [1 + e^{E_B} V_1 f(d, l_0)]}{r_{\text{DBD}} [1 + e^{E_B} V_1 f(d, l_0)] + r_{\text{IDR}} + 1}, \quad (3)$$

where $r_{\text{DBD}} \equiv \nu e^{E_{\text{DBD}}}$ and $r_{\text{IDR}} \equiv \nu e^{E_B}$. Note that r_{DBD} and r_{IDR} are much smaller than 1 in reality. To understand the contribution of the IDR, we compare P_{TF} to the probability of a “simple” TF, composed of a single DBD site, where $P_{\text{IDR}} = P_{\text{both}} = 0$. Thus, $P_{\text{simple}} = r_{\text{DBD}}/(r_{\text{DBD}} + 1)$. The ratio $P_{\text{TF}}/P_{\text{simple}}$ indicates the enhancement in binding affinity due to the presence of the IDR, and is given by:

$$\frac{P_{\text{TF}}}{P_{\text{simple}}} = \frac{1 + r_{\text{DBD}}}{r_{\text{DBD}} + (1 + r_{\text{IDR}})(1 + \mathcal{P})^{-1}} \approx 1 + \mathcal{P}, \quad (4)$$

where $\mathcal{P} = e^{E_B} V_1 f(d, l_0)$ is an enhancement factor of one more IDR site bound to the targets. The approximation derives from $\mathcal{P} \ll 1/r_{\text{DBD}}$, which is the case in our scenario. \mathcal{P} represents the trade-off between the gain in IDR binding energy, denoted as E_B , and the loss of entropy, represented by $\ln(V_1 f(d, l_0))$. If $\mathcal{P} \ll 1$, adding IDR sites will not significantly increase the binding probability. The exponential decay of \mathcal{P} with d^2 indicates that a compact target placement is preferable. However, due to the physical limitations, d cannot be arbitrarily small and has a lower bound. Once d is fixed, from Eq. (4), \mathcal{P} is maximal at $l_0 = d$. It indicates that the distance between IDR binding sites should be comparable to the distance between targets for an optimal design. This requirement is also effective when multiple IDR sites and targets are involved. See the verification in Fig. 2(a).

We set $d = l_0$ and investigate other parameters that characterize the TF search. Such quantities are E_B , the number of IDR sites, n_b , and the number of corresponding targets along the DNA, M . The generalization requires taking into account all the possible number of bindings, n from 0 to $\min(n_b, M)$, and all possibilities for binding orientations for each n . Consider a given configuration, where IDR sites $q_1 < \dots < q_n$ are bound to targets s_1, \dots, s_n . We will denote the DBD site by $q_0 = 0$ and its target by $s_0 = 0$. The typical distance between sites q_{i-1} and q_i in the unbound state is given by $l_{\text{orn},i} = \sqrt{q_i - q_{i-1}} l_0$, as can be seen from Eq. (1). The corresponding targets distance is $r_{\text{orn},i} = |s_i - s_{i-1}| d$. Eq. (2c) describes the probability for both the DBD and IDR to be bound, for the case of an IDR containing only one binding site. Similarly, for the case of an IDR with n_b binding sites, we can find the probability to have $n \leq n_b$ IDR sites bound (in addition to the DBD), which we find to be proportional to $r_{\text{DBD}} \prod_{i=1}^n \mathcal{P}(r_{\text{orn},i}, l_{\text{orn},i})$

where $\mathcal{P}(r_{\text{orn},i}, l_{\text{orn},i}) = e^{E_B} V_1 f(r_{\text{orn},i}, l_{\text{orn},i})$. Thus, the total binding probability is proportional to $r_{\text{DBD}} (1 + \sum_n \sum_{\text{orn}} \prod_{i=1}^n \mathcal{P}(r_{\text{orn},i}, l_{\text{orn},i}))$, where “orn” stands for $\binom{n_b}{n} \binom{M}{n} n!$ possible binding orientations at n . See the derivation P_{TF} in S1 of the Supplemental Material (SM). We investigated the ratio $P_{\text{TF}}/P_{\text{simple}}$ obtained by all possible combinations of $n_b \in \{1, 2, \dots, 11\}$ and $M \in \{1, 2, \dots, 12\}$. In Fig. 2(b) we present the maximal ratio $P_{\text{TF}}^*/P_{\text{simple}}$ across n_b and M when varying E_B . At small E_B , because $\mathcal{P} < 1$, adding IDR sites does not help increase the ratio significantly and the ratio is ~ 1 . At large E_B , for some orientations since $\mathcal{P} > 1$, the ratio is much larger than 1 and saturates as P_{TF}^* approaches 1. For intermediate E_B , the ratio increases very rapidly. The corresponding typical E_{th} could be estimated by the formula

$$\mathcal{P} = e^{E_{\text{th}}} V_1 f(d, d) \approx 1, \quad (5)$$

which corresponds to the contribution of binding orientations that are associated with the least loss of entropy. The vertical dashed line in Fig. 2(b), obtained from Eq. (5), captures this feature well. In Fig. 2(c) we show the heat map of $P_{\text{TF}}/P_{\text{simple}}$ at different n_b and M . As n_b decreases, the value of P_{TF} exhibits a substantial decrease, following an initial slow decay. It is reminiscent of the observations from experiments in Ref. [9], wherein the binding specificity decreases rapidly after a gradual decay with decreasing length of the IDR. The orange contour line corresponds to a binding probability $P_{\text{TF}} = 0.9$. In Fig. 2(d), we display the contour lines at different E_B at the value of $P_{\text{TF}} = 0.9$. The minimal number of binding sites (n_b^*) and targets (M^*) required to achieve this value are represented by blue dots. We find that n_b^* is comparable to M^* and that n_b^* decreases with increasing E_B as displayed in the inset. These relationships also hold at $P_{\text{TF}} = 0.5$ (see S2 for details).

So far, we have found that the optimality binding principles for TFs with IDRs are as follows: (a) target distance d should be as small as possible. (b) IDR segment binding distance l_0 should be comparable to d , (c) IDR binding strength E_B should be larger than a threshold (indicated by Eq. (5)), and (d) it is preferable to have fewer binding sites n_b^* and binding targets M^* as the binding strength E_B increases, and n_b^* is comparable to M^* .

Search time of the TF from the dynamics— In this section, we study the design principles of the TF search time, a dynamic process. Here, we confine the TF with $\tilde{n} \equiv n_b + 1$ sites (n_b IDR sites and one DBD site) to a sphere of radius R , the cell nucleus, and use over-damped molecular dynamics (MD) simulations. The sites and targets interact via a short-range interaction. The DBD target with a radius a is placed at the sphere’s center. See the sketch in Fig. 1(b). Once the DBD finds its target, the search ends. The total search time, denoted as t_{total} ,

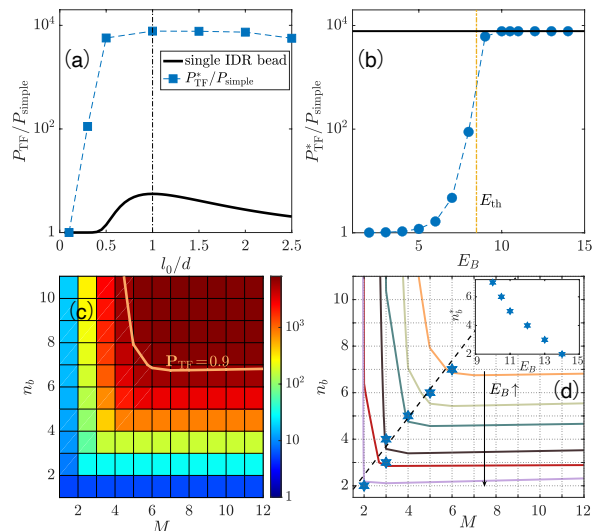


Figure 2. (a) The ratio $P_{\text{TF}}/P_{\text{simple}}$ for typical values of the relevant quantities: the nucleus volume is $1\mu\text{m}^3$, $E_{\text{DBD}} = 15$, $E_B = 10$, $V_1 = (0.34\text{nm})^3$, and $d = \sqrt{50} \cdot 0.34\text{nm}$. The black solid line corresponds to a TF with a single IDR site. The blue dots correspond to the maximal ratio across $n_b \in [1, 11]$ and $M \in [1, 12]$, where maximal P_{TF} is denoted by P_{TF}^* . (b) $P_{\text{TF}}^*/P_{\text{simple}}$ for varying E_B at $d=l_0$. The dashed vertical line corresponds to E_{th} obtained from Eq. (5), and the solid horizontal line is where $P_{\text{TF}} = 1$. (c) A heat map demonstrating the variations in $P_{\text{TF}}/P_{\text{simple}}$ for different combinations of n_b and M at $E_B = 10$ and $d=l_0$. The contour line is at the binding probability $P_{\text{TF}} = 0.9$. (d) Contour lines at different E_B at $P_{\text{TF}} = 0.9$. Blue dots represent the minimal number of binding sites (n_b^*) and targets (M^*) required to achieve this value of P_{TF} , where M^* and n_b^* are integers. The black dashed line is a visual guide, illustrating the relationship $n_b^* \sim M^*$. The inset: n_b^* decreases as E_B increases.

is obtained by averaging on 500 independent equilibrium configurations of the TF, each starting from a random position. The corresponding result is called the mean first passage time (MFPT). The span length of targets along the DNA is $L \equiv Md$. We use an adaptive time step. See details of the simulations in S3.

By conducting comprehensive simulations of t_{total} across various parameter values of L , E_B , and \tilde{n} , we were able to identify its minimum value, which is approximately at $L^* = 300\text{bp}$, $E_B^* = 11$, and $\tilde{n}^* = 4$ for $R = 500\text{bp} \approx 1/6\mu\text{m}$. Here one base pair (bp) is equal to 0.34nm . The acquisition of these results required about 10^5 CPU hours. The probability distribution function (pdf) of individual search times exponentially decays with a typical time equal to the MFPT t_{total} , see inset of Fig. 3(b), which means t_{total} is a good representation of the search time.

We find that t_{total} non-monotonically varies with L at fixed E_B^* and \tilde{n}^* as shown in Fig. 3. Once a TF attaches to one of its targets, it will most likely diffuse along the DNA until reaching the DBD target (see S4 for details).

It means that the optimal search process is a single round of 3D diffusion followed by 1D diffusion along the DNA. The 3D search time, t_{3D} , and the 1D search time, t_{1D} , are shown in Fig. 3. t_{3D} is reminiscent of the MFPT of a particle hitting an extremely thin ellipsoid, which is proportional to $\ln(L/r_p)/L$, where L represents the length of the major axis and r_p represents the length of the semi-minor axis [21]. In our case, $r_p = \sqrt{\tilde{n}/6}l_0$ is the radius of gyration of the TF polymer, and when the distance between the TF and the DNA is smaller than r_p , then the TF would most probably attach to the targets. r_p is larger than the target distance d but much smaller than L . So, it is possible to think about the DNA segment where the targets reside as an effective target that is bigger than the simple sum of the individual target sizes, which is often referred to as an ‘‘antenna’’ effect [12, 22, 23]. For the 1D search from a single particle picture, since the TF is unlikely to detach once it attaches, it performs a 1D random walk with reflecting boundaries at the end of the targets’ domain. So, all in all, the total search time is

$$t_{\text{total}} = t_{3D} + t_{1D} \approx \frac{\alpha \tilde{n} R^3}{DL} \ln(L/r_p(\tilde{n})) + \frac{\tilde{n} L^2}{\pi^2 c D}, \quad (6)$$

where D is the 3D diffusion coefficient of one site. For a TF with \tilde{n} sites, its 3D diffusion coefficient, D_3 , is D/\tilde{n} , and effective 1D diffusion coefficient, D_1 , is cD/\tilde{n} . α and c are fitting parameters. The semi-analytical formulas of t_{1D} , t_{3D} , and t_{total} denoted by the solid lines in Fig. 3 agree well with the simulation results at $\alpha = 0.5$ and $c = 0.028$. The theoretical result for the time spent in 3D was originally calculated for a point searcher [21]. In that case, a value of $\alpha = 2/3$ was obtained. The parameter c is dependent on both E_B and \tilde{n} , and will be discussed in the following section.

We also checked Eq. (6) vs. E_B and vs. \tilde{n} around (L^*, \tilde{n}^*) and (L^*, E_B^*) , respectively (see the plots in S5). When $E_B > E_B^*$, t_{3D} is a constant with $\alpha = 0.5$, and t_{1D} (or c) exponentially decreases with increasing E_B since the dwelling time on the different targets exponentially increases with E_B , similar to the effect of roughness of energy landscapes (the fluctuation of the binding energy) discussed in Ref. [24]. When $E_B < E_B^*$, Eq. (6) breaks down because of multiple rounds of hits on the DNA before reaching the DBD target. For \tilde{n} , when $\tilde{n} > \tilde{n}^*$, t_{3D} agrees with the prediction, and t_{1D} is insensitive to \tilde{n} . See S5 for further details. Interestingly, when we observe the motion of a TF along the DNA, it is like an octopus where IDR sites are like its ‘‘tentacles’’ as illustrated in Fig. 1(c). We refer to this 1D walk as ‘‘octopusing’’, inspired by the famous ‘‘reptation’’ motion in entangled polymers suggested by de Gennes [25]. The binding and unbinding of IDR sites on the DNA satisfies the detailed balance where the off-rate of sites equals the on-rate. However, when $\tilde{n} < \tilde{n}^*$, the TF has fewer ‘‘tentacles’’, and it cannot walk a long distance along the DNA,

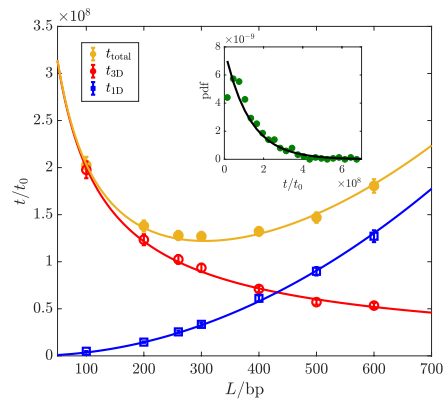


Figure 3. t_{total} , t_{3D} and t_{1D} vs. L at E_B^* and \tilde{n}^* . The solid fitting curves (red and blue) correspond to the parameters $\alpha = 0.5$ and $c = 0.028$. Inset: probability density function (pdf) exponentially decays at large t . $\text{pdf} \approx \exp(-t/t_{\text{total}})/t_{\text{total}}$ (black solid line). The unit t_0 represents the time for one AA to diffuse 1bp. $a = 0.5$ bp, $d = 10$ bp, and $l_0 = 5$ bp.

which implies the affinity of TF to DNA decreases with \tilde{n} . As a consequence, multiple rounds of 3D-1D random walks are needed to reach the DBD target, and the search time dramatically increases with decreasing \tilde{n} . We also found that the 1D ‘‘octopusing’’ walk is swift at small E_B where $c \approx 0.5$. See the extended discussion in S6.

Clearly, a simple TF without an IDR cannot make use of the neighboring IDR targets to walk along the DNA. The minimal search time for such a TF is $t_{\text{simple}} = R^3/(3Da)$ [21]. For the TF with an IDR, the minimal search time t_{min} at $R = 500$ bp is about 16 times shorter than a simple TF, although the latter’s diffusion coefficient is four times larger. The real radius of the nucleus is about $1\mu\text{m}$ which is about six times larger than the value used in Fig. 3. Due to the limitation of computing time, we cannot systematically run the simulations in this case. However, by neglecting the logarithmic term’s slow variation with respect to L in Eq. (6), we can approximate $t_{\text{min}} \sim c^{-1/3}R^2$. It leads to the optimal $L \sim c^{-1/6}R$, which should increase with increasing R despite decreasing c . Therefore, a larger R will lead to a more significant speed-up. Although the persistence length of the DNA is several-fold shorter than the optimal L , the qualitative results would still hold, and the speed-up factor can reach magnitudes of several dozens.

Discussion— In this work, we addressed the optimal design principles of TFs containing IDRs, with respect to binding specificity and search time. We find that both parameters are significantly enhanced compared to simple TFs lacking IDRs. Regarding binding specificity, we have observed that the binding probability is highly influenced by the distance d between targets on DNA and the binding strength E_B . Maximal binding probability P_{TF}^* requires that the distance l_0 between the binding sites along the IDR would be comparable to d , and the opti-

mal number of targets M^* is comparable to the optimal number of binding sites n_b^* . Both M^* and n_b^* decrease as E_B increases. Regarding the search dynamics, TFs with IDRs are capable of random walking along the binding targets domain of the DNA, leading to a significant decrease in search time when compared to a single DBD target, which as mentioned earlier is often referred to as an “antenna” effect [12, 22, 23]. We find that the minimal search time t_{\min} corresponds to one round of 3D-1D search, and the optimal binding targets domain length L^* can be found by a semi-analytical expression. t_{\min} is comparable to its 3D search time t_{3D} with a ratio between 1 to 1.5 (ignoring the logarithmic correction in t_{3D} yields a ratio of 1.5.). Note that the minimal search time t_{\min} in a single round of 3D-1D search process is significantly shorter compared to the minimal search time obtained when multiple rounds of 3D-1D excursions take place, as in the facilitated diffusion (FD) model [10–15]. See the details in S7.

The simplified model we presented provides general design principles for the search process and testable predictions. One possible experiment that could shed light on one of our key assumptions is “scrambling” the DNA (randomizing the order of nucleotides). Our results depend greatly on our assumption that there exists a region on the DNA, close to the DBD target, that contains targets for the IDR binding sites. It is possible to shuffle, or even remove, regions of different lengths around the DBD target and to measure the resulting changes in binding affinity. According to our results, We would expect that shuffling a region smaller in length than the IDR (or shorter) should have minimal effect on the binding affinity and search time, but that shuffling a region longer than the IDR should have a noticeable effect.

Another useful test of our model would be to probe the *dynamics* of the TF search process by varying the waiting time before TF-DNA interactions are measured: Within the ChEC-seq technique [26] employed in [9], an enzyme capable of cutting the DNA is attached to the TF, and activated at will (using an external calcium signal). Sequencing then informs us of the places on the DNA at which the TF was bound at the point of activation. Measuring the binding probabilities at various waiting times, ranging from seconds to an hour, would inform us both of the TF search dynamics as well as the equilibrium properties: Shorter time scales would capture the dynamics of the search process, while longer time scales would reveal the equilibrium properties of the binding. According to our results, the binding probability of TFs with IDRs will display significant variations across different waiting times, whereas TFs without IDRs will be less influenced. After a prolonged duration, both binding probabilities will reach their saturation values, with TFs with IDRs having a significantly higher value than those without IDRs.

In the future, it would be interesting to explore the

possible role of TF-TF interactions as well as the complex DNA conformation, considered in some previous studies of the facilitated diffusion model [27, 28]. It would also be useful to study the molecular basis for the TF-DNA binding, which we addressed here within a coarse-grained model.

Acknowledgments We thank Samuel Safran, David Mukamel, Yariv Kafri, Luyi Qiu, and Zily Burstein for insightful discussions. We thank the Clore Center for Biological Physics for their generous support.

-
- [1] J. Liu, N. B. Perumal, C. J. Oldfield, E. W. Su, V. N. Uversky, and A. K. Dunker, *Biochemistry* **45**, 6873 (2006).
 - [2] M. Fuxreiter, I. Simon, and S. Bondos, *Trends in Biochemical Sciences* **36**, 415 (2011).
 - [3] X. Guo, M. L. Bulyk, and A. J. Hartemink, in *Biocomputing 2012* (World Scientific, 2012) pp. 104–115.
 - [4] P. E. Wright and H. J. Dyson, *Nature Reviews Molecular Cell Biology* **16**, 18 (2014).
 - [5] J. T. Kadonaga, A. J. Courey, J. Ladika, and R. Tjian, *Science* **242**, 1566 (1988).
 - [6] A. J. Courey, D. A. Holtzman, S. P. Jackson, and R. Tjian, *Cell* **59**, 827 (1989).
 - [7] D. Vuzman and Y. Levy, *Proceedings of the National Academy of Sciences* **107**, 21004 (2010).
 - [8] D. Vuzman and Y. Levy, *Molecular Biosystems* **8**, 47 (2012).
 - [9] S. Brodsky, T. Jana, K. Mittelman, M. Chapal, D. K. Kumar, M. Carmi, and N. Barkai, *Molecular Cell* **79**, 459 (2020).
 - [10] O. G. Berg, R. B. Winter, and P. H. Von Hippel, *Biochemistry* **20**, 6929 (1981).
 - [11] O. G. Berg and P. H. von Hippel, *Journal of Molecular Biology* **193**, 723 (1987).
 - [12] L. Mirny, M. Slutsky, Z. Wunderlich, A. Tafvizi, J. Leith, and A. Kosmrlj, *Journal of Physics A: Mathematical and Theoretical* **42**, 434013 (2009).
 - [13] G.-W. Li, O. G. Berg, and J. Elf, *Nature Physics* **5**, 294 (2009).
 - [14] O. Bénichou, C. Loverdo, M. Moreau, and R. Voituriez, *Reviews of Modern Physics* **83**, 81 (2011).
 - [15] M. Sheinman, O. Bénichou, Y. Kafri, and R. Voituriez, *Reports on Progress in Physics* **75**, 026601 (2012).
 - [16] P. Hammar, P. Leroy, A. Mahmutovic, E. G. Marklund, O. G. Berg, and J. Elf, *Science* **336**, 1595 (2012).
 - [17] T. Jana, S. Brodsky, and N. Barkai, *Trends in Genetics* **37**, 421 (2021).
 - [18] J. J. Ferrie, J. P. Karr, R. Tjian, and X. Darzacq, *Molecular Cell* (2022).
 - [19] P. E. Rouse Jr, *The Journal of Chemical Physics* **21**, 1272 (1953).
 - [20] M. Doi and S. F. Edwards, *The Theory of Polymer Dynamics*, Oxford University Press (1988).
 - [21] H. C. Berg, in *Random Walks in Biology* (Princeton University Press, 2018).
 - [22] N. Shimamoto, *Journal of Biological Chemistry* **274**, 15293 (1999).

- [23] M. Castellanos, N. Mothi, and V. Muñoz, *Nature Communications* **11** (2020).
- [24] M. Slutsky and L. A. Mirny, *Biophysical Journal* **87**, 4021 (2004).
- [25] P. De Gennes and L. Leger, *Annual Review of Physical Chemistry* **33**, 49 (1982).
- [26] G. E. Zentner, S. Kasinathan, B. Xin, R. Rohs, and S. Henikoff, *Nature Communications* **6** (2015).
- [27] T. Hu, A. Y. Grosberg, and B. Shklovskii, *Biophysical Journal* **90**, 2731 (2006).
- [28] M. A. Lomholt, B. van den Broek, S.-M. J. Kalisch, G. J. Wuite, and R. Metzler, *Proceedings of the National Academy of Sciences* **106**, 8204 (2009).
- [29] J. D. Weeks, D. Chandler, and H. C. Andersen, *The Journal of Chemical Physics* **54**, 5237 (1971).
- [30] Z. Wunderlich and L. A. Mirny, *Nucleic Acids Research* **36**, 3570 (2008).
- [31] O. Hachmo and A. Amir, *arXiv:2209.00500* (2022).
- [32] I. Leven and Y. Levy, *Nucleic Acids Research* **47**, 5530 (2019).
-

Supplemental material for Roles of intrinsically disordered regions in transcription factor search

S1. Derivation for the binding probability

In this section, we derive the generalized binding probability P_{TF} for n_b IDR binding sites and M IDR targets. To achieve this generalization, we consider all the possible number of bindings, n from 0 to $\min(n_b, M)$, and all possibilities for binding orientations for each n .

Based on the Rouse model, the system's energy can be expressed as $\frac{k}{2} \sum_{i=1}^{n_b} (\vec{r}_i - \vec{r}_{i-1})^2 = \frac{3k_B T}{2l_0^2} \sum_{i=1}^{n_b} (\vec{r}_i - \vec{r}_{i-1})^2$, where \vec{r}_i represents the position of the binding site i . The probability density in the absence of binding reads:

$$\rho(\vec{r}_0, \dots, \vec{r}_{n_b}) = \frac{1}{V_c} \left(\frac{3}{2\pi l_0^2} \right)^{\frac{3}{2}n_b} e^{-\frac{3}{2l_0^2} \sum_{i=1}^{n_b} (\vec{r}_i - \vec{r}_{i-1})^2}, \quad (\text{S1})$$

where $\int d^3 \vec{r}_0 \dots \int d^3 \vec{r}_{n_b} \rho(\vec{r}_0, \dots, \vec{r}_{n_b}) = 1$.

Now we consider a given configuration with n IDR sites bound, where IDR sites $q_1 < \dots < q_n$ are bound to targets s_1, \dots, s_n . The positions of these bound targets are at $\vec{R}_{s_1}, \dots, \vec{R}_{s_n}$. The DBD site is denoted by $q_0 = 0$ and its target is denoted by $s_0 = 0$. There are $n_b - n$ unbound IDR sites, indicated by $\bar{q}_1 < \dots < \bar{q}_{n_b-n}$. The corresponding binding probability is given by:

$$P_{\text{bound}}(\text{orn}, n) = \frac{1}{Z} \prod_{i=0}^n \int_{\vec{r}_{q_i} \in V_1} d^3 \vec{r}_{q_i} \prod_{\ell=1}^{n_b-n} \int_{\vec{r}_{\bar{q}_\ell} \notin V_1} d^3 \vec{r}_{\bar{q}_\ell} \rho(\vec{r}_0, \dots, \vec{r}_{n_b}) e^{E_{\text{DBD}} + nE_B}, \quad (\text{S2})$$

where ‘‘orn’’ stands for the orientation of the given configuration, Z is the normalization factor. There are $\binom{n_b}{n} \binom{M}{n} n!$ possible binding orientations at n . The key insight in evaluating this integral is to realize that we can use the result of Eq. (1) of the main text to integrate out the degrees of freedom associated with the sites between q_{i-1} and q_i :

$$\prod_{\bar{q}_\ell=q_{i-1}+1}^{\bar{q}_\ell=q_i-1} \left[\int d^3 \vec{r}_{\bar{q}_\ell} \left(\frac{3}{2\pi l_0^2} \right)^{3/2} \exp \left(-\frac{3(\vec{r}_{\bar{q}_\ell} - \vec{r}_{\bar{q}_{\ell-1}})^2}{2l_0^2} \right) \right] = f(|\vec{r}_{q_i} - \vec{r}_{q_{i-1}}|, \sqrt{q_i - q_{i-1}} l_0). \quad (\text{S3})$$

Since $r_{q_{i-1}}$ and r_{q_i} are confined to a very small volume V_1 , to an excellent approximation we may simply evaluate $f(|\vec{r}_{q_i} - \vec{r}_{q_{i-1}}|, \sqrt{q_i - q_{i-1}} l_0)$ in Eq. (S3) at $\vec{r}_{q_{i-1}} = \vec{R}_{s_{i-1}}$ and $\vec{r}_{q_i} = \vec{R}_{s_i}$, to obtain:

$$P_{\text{bound}}(\text{orn}, n) \simeq \frac{1}{Z} \frac{V_1^{n+1}}{V_c} \prod_{i=1}^n f(|s_i - s_{i-1}| d, \sqrt{q_i - q_{i-1}} l_0) e^{E_{\text{DBD}} + nE_B} = \frac{1}{Z} r_{\text{DBD}} \prod_{i=1}^n \mathcal{P}(r_{\text{orn},i}, l_{\text{orn},i}), \quad (\text{S4})$$

where $r_{\text{DBD}} = \frac{V_1}{V_c} e^{E_{\text{DBD}}}$, $r_{\text{orn},i} = |s_i - s_{i-1}| d$, $l_{\text{orn},i} = \sqrt{q_i - q_{i-1}} l_0$, and $\mathcal{P}(r_{\text{orn},i}, l_{\text{orn},i}) = e^{E_B} V_1 f(r_{\text{orn},i}, l_{\text{orn},i})$.

To give a specific example, consider the binding topology corresponding to Fig. S1. In this case, $n = 3$, $l_{\text{orn},1} = l_0$ (since there is one spring between the DBD and the first binding site), $l_{\text{orn},2} = \sqrt{3} l_0$ (since there are 3 springs between q_1 and q_2) and similarly $l_{\text{orn},3} = l_0$. Eq. (S3) implies that the contribution of this diagram to the binding probability is: $\frac{1}{Z} \frac{V_1^4}{V_c} \frac{27}{(2\pi l_0^2)^{9/2}} e^{3E_B + E_{\text{DBD}} - 5d^2/l_0^2}$. Note that while in this example the order of the target sites is monotonic (i.e., as we increase the index of the binding sites, we progressively move further away from the DBD), in principle we should sum over *all* diagrams, including those where the order is non-monotonic.

At $n = 0$, $P_{\text{bound}}(\text{orn}, 0) = \frac{1}{Z} r_{\text{DBD}}$.

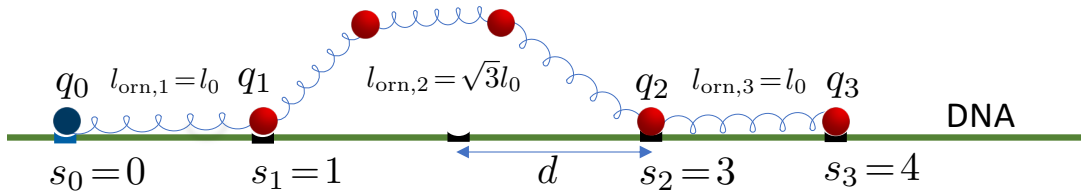


Figure S1. A diagram of the bound configurations at $n = 3$.

Similarly, for the state where the DBD is unbound and $n \geq 2$ IDR sites are bound, the binding probability reads:

$$P_{\text{unbound}}(\text{orn}, n) = \frac{1}{Z} \int_{\vec{r}_0 \notin V_1} d^3 \vec{r}_0 \prod_{\ell=1}^n \int_{\vec{r}_{q\ell} \in V_1} d^3 \vec{r}_{q\ell} \prod_{\ell=1}^{n_b-n} \int_{\vec{r}_{i\ell} \notin V_1} d^3 \vec{r}_{i\ell} \rho(\vec{r}_0, \dots, \vec{r}_{n_b}) e^{nE_B} \simeq \frac{1}{Z} r_{\text{IDR}} \prod_{i=2}^n \mathcal{P}(r_{\text{orn},i}, l_{\text{orn},i}), \quad (\text{S5})$$

where $r_{\text{IDR}} = \frac{V_1}{V_c} e^{E_B}$. For $n=1$, $P_{\text{unbound}}(\text{orn}, 1) = \frac{Mn_b}{Z} r_{\text{IDR}}$. Here Mn_b represents the number of possibilities for one of the n_b IDR sites bound to one of the M targets. For $n=0$, $P_{\text{unbound}}(\text{orn}, 0) = \frac{1}{Z} \prod_{i=0}^{n_b} \int_{\vec{r}_i \notin V_1} d^3 \vec{r}_i \rho(\vec{r}_0, \dots, \vec{r}_{n_b}) \simeq \frac{1}{Z}$.

Since the sum of all the possibilities is equal to 1, as given by: $\sum_{n=0}^{\min\{n_b, M\}} \sum_{\text{orn}} (P_{\text{bound}} + P_{\text{unbound}}) = 1$, we can determine the normalization factor. Therefore, the binding probability P_{TF} for the DBD bound in its target can be expressed as:

$$P_{\text{TF}} = \frac{r_{\text{DBD}} \left(1 + \sum_{n=1}^{\min\{n_b, M\}} \sum_{\text{orn}} \sum_{i=1}^n \mathcal{P}(r_{\text{orn},i}, l_{\text{orn},i}) \right)}{r_{\text{DBD}} \left(1 + \sum_{n=1}^{\min\{n_b, M\}} \sum_{\text{orn}} \sum_{i=1}^n \mathcal{P}(r_{\text{orn},i}, l_{\text{orn},i}) \right) + 1 + r_{\text{IDR}} \left(Mn_b + \sum_{n=2}^{\min\{n_b, M\}} \sum_{\text{orn}} \sum_{i=2}^n \mathcal{P}(r_{\text{orn},i}, l_{\text{orn},i}) \right)}. \quad (\text{S6})$$

At $n_b = M = 1$, the general formula above returns to Eq. (3) in the main text.

S2. Robustness of the relationships: $n_b^* \sim M^*$ and n_b^* decreases with increasing E_B

Fig. S2 shows the contour lines at $P_{\text{TF}}=0.9$ and $P_{\text{TF}}=0.5$. The relationship between the minimal number of sites (n_b^*) and targets (M^*) needed to achieve $P_{\text{TF}} = 0.5$ and $P_{\text{TF}} = 0.9$ demonstrates consistent linearity, guided by the black dashed line. It indicates the robustness of the relationship for $n_b^* \sim M^*$. At $P_{\text{TF}} = 0.5$, the relationship where n_b^* decreases as E_B increases also holds.

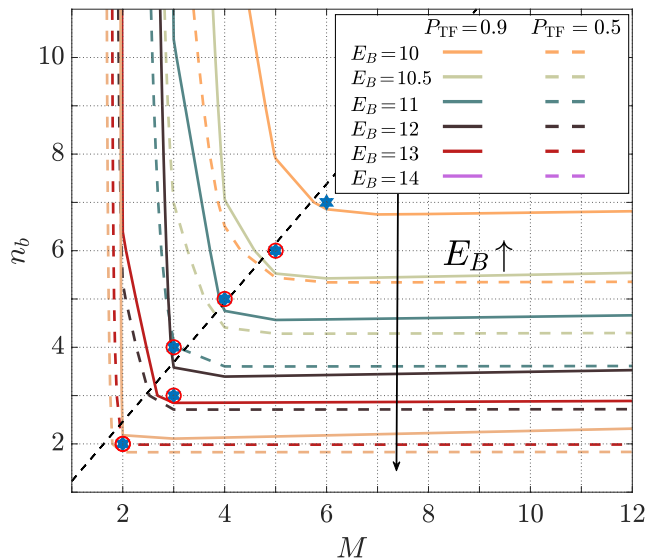


Figure S2. Contour lines at $P_{\text{TF}}=0.9$ and $P_{\text{TF}}=0.5$ on the plane defined by the number of binding sites, n_b , and the number of binding targets, M . (M^*, n_b^*) at different E_B are denoted by blue hexagams at $P_{\text{TF}}=0.9$ and red circles at $P_{\text{TF}}=0.5$. The black dashed line is added to guide the relationship $n_b^* \sim M^*$.

S3. Dynamical simulations

Each binding site of the TF at position \mathbf{r}_i follows over-damped dynamics, which reads:

$$d\mathbf{r}_i = \frac{D}{k_B T} \mathbf{f}(\{\mathbf{r}_i\}) dt + \sqrt{2Ddt} \xi, \quad (\text{S7})$$

where the random variable ξ follows the standard normal distribution. The force acting on each site is $\mathbf{f}(\{\mathbf{r}_i\}) \equiv -\partial U_{\text{total}}/\partial \mathbf{r}_i$, and

$$U_{\text{total}} = \sum_{i=0}^{n_b-1} \frac{1}{2} k (\mathbf{r}_{i+1} - \mathbf{r}_i)^2 + \sum_j E_B \exp \left[-\frac{(\mathbf{r}_i - \mathbf{R}_j)^2}{2w_d^2} \right], \quad (\text{S8})$$

where \mathbf{R}_j are the positions of the targets. $w_d = 1$ bp is the typical width of the short-range interaction between sites and their corresponding targets. Here we consider the DBD interaction with the IDR targets as well. To speed up the MD simulations, when the sites' minimal distance to the DNA is larger than the threshold 10bp, the TF is regarded as a rigid body, and all sites move in sync with their center of mass. We verified that the resulting search time is insensitive to the value of this threshold. When the sites' minimal distance to the DNA is less than 10 bp, we consider the excluded volume effect to ensure that different binding sites are not trapped at the same target. Specifically, we use the WCA interaction [29]:

$$U_{\text{WCA}} = \begin{cases} \frac{\sigma^{12}}{|\mathbf{r}_i - \mathbf{r}_j|^{12}} - \frac{2\sigma^6}{|\mathbf{r}_i - \mathbf{r}_j|^6} + 1, & |\mathbf{r}_i - \mathbf{r}_j| < \sigma \\ 0, & |\mathbf{r}_i - \mathbf{r}_j| \geq \sigma \end{cases}, \quad (\text{S9})$$

where $\sigma = 1$ bp. In this region, we also adopted an adaptive time step which reads

$$\frac{dt}{\text{bp}^2/D} = \min \left\{ 1, \frac{1}{\max |\mathbf{f}_i| \text{ bp}} \right\} \times 0.01. \quad (\text{S10})$$

Note that this choice ensures that the displacement of the sites at every step is smaller than 0.01bp that is much smaller than w_d .

S4. TF walking along the DNA once it attaches to IDR targets

We show a typical example of the trajectory of a TF (red) in the cell nucleus (light blue) in Fig. S3(a) where the TF walks along the DNA to the DBD target once it attaches the IDR targets at \tilde{n}^* and E_B^* . The DBD target is at the origin. In Fig. S3(b), we find that the average number of rounds the TF hits the DNA, n_{hits} , is close to 1 so it is fair to describe the overall search process as two distinct steps with the first step being purely a 3D search and the second a purely 1D search. This is expressed by Eq.(6) in the main text.

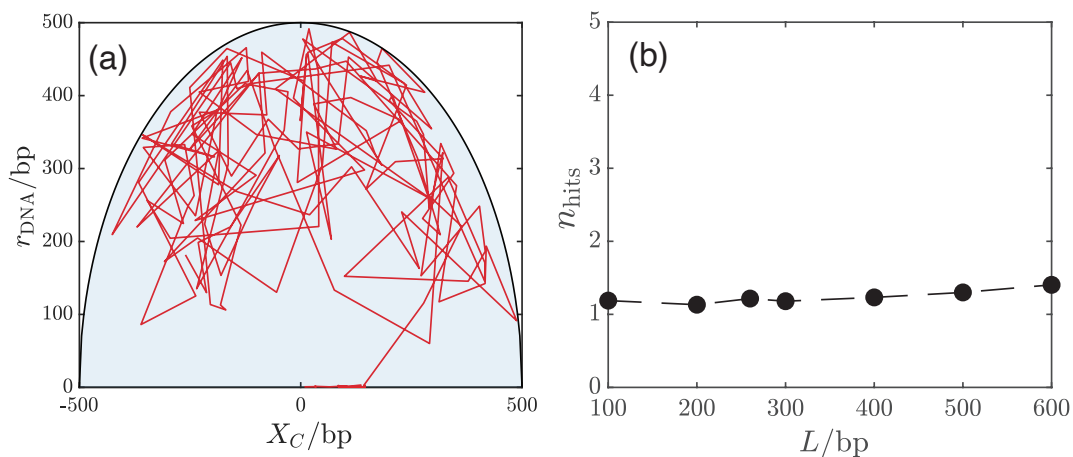


Figure S3. (a) A trajectory (red) of TF in the cell nucleus (light blue). r_{DNA} is the average distance of the TF to the DNA and X_c is the position of the center of mass along the DNA direction. The trajectory is displayed with a time interval of $10^6 t_0$. (b) The average number of rounds the TF hits the DNA, n_{hits} , before reaching the DBD target.

S5. Search time t_{total} vs. E_B and vs. \tilde{n}

Fig. S4 (a) shows t_{total} vs. E_B . When $E_B > E_B^*$, t_{3D} does not depend on E_B as we predict (red solid line) and t_{1D} (the parameter c) exponentially decreases (increases) with increasing E_B . The solid blue line, also shown in the inset, fits with the form $\propto \exp(0.47E_B)$. At $E_B < E_B^*$, since the number of rounds of hits on DNA, n_{hits} , is significantly larger than 1, as displayed in the inset, Eq. (6) breaks down.

Fig. S4 (b) shows t_{total} vs. \tilde{n} . When $\tilde{n} > \tilde{n}^*$, t_{3D} agrees with the prediction (red curve). t_{1D} exhibits weak dependence on \tilde{n} , implying a linear increase of c with \tilde{n} here. Generally, the relationship between c and \tilde{n} also depends on E_B . When $\tilde{n} < \tilde{n}^*$, Eq. (6) in the main text breaks down because of multiple rounds of hits, which is verified in the inset. t_{3D} dramatically increases with decreasing \tilde{n} because of the increase in n_{hits} . It suggests that the 1D mean diffusion distance L/n_{hits} decreases with decreasing E_B . If each round of 3D search is independent, the 3D search time should be n_{hits} times the one round of 3D search time (red solid curve), displayed in the black curve. However, the black curve is above the red dots, which implies that the successive 3D random walks are correlated.

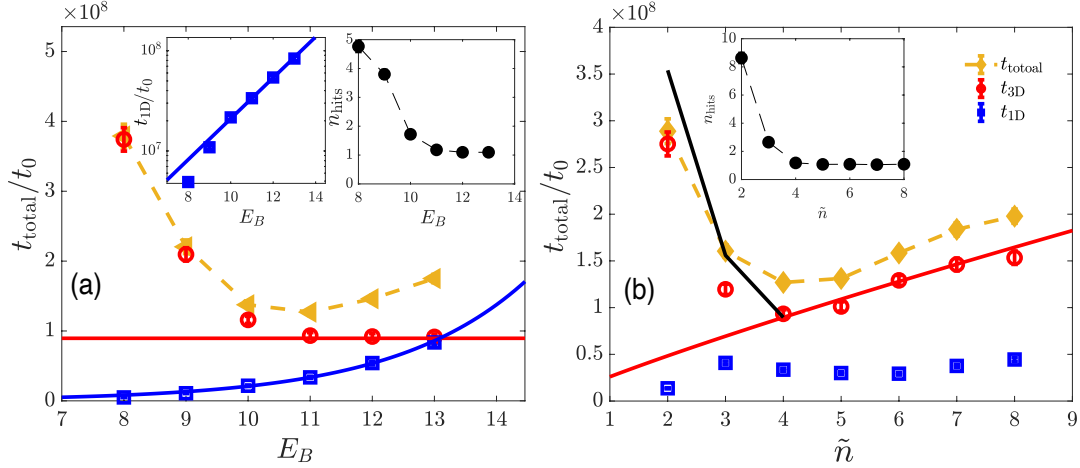


Figure S4. (a) t_{total} , and decomposed t_{3D} and t_{1D} vs. E_B at L^* and \tilde{n}^* . The red solid line is the prediction with $\alpha = 0.5$, and the blue line (also in the inset) is the exponential increase fit. The black curve in the inset is the number of rounds the TF hits the DNA, n_{hits} , vs. E_B . (b) t_{total} , t_{3D} , and t_{1D} vs. \tilde{n} at L^* and E_B^* . The red solid line is the prediction of t_{3D} as a function of \tilde{n} from Eq. (6). n_{hits} varying with \tilde{n} is shown in the inset.

S6. Properties of Octopusing

To specifically study how the length of the TF, namely \tilde{n} , determines the 1D “octopusing” walk, we study the time spent by the TF prior to falling off the DNA, t_{detach} . The TF is initially on the DNA. Here, we set $E_B = 6$, which is smaller than the optimal E_B^* and allows us to have a big range of \tilde{n} to see the off-time dependence under our computing time limit. From Fig. S5(a), we see that t_{detach} exponentially increases with \tilde{n} , which suggests that the effective trapped potential for the TF on the DNA is proportional to \tilde{n} , and that binding affinity is significantly enhanced. t_{detach} is averaged over 100 independent configurations. The inset of Fig. S5(a) shows the probability distribution of the time spent for individual configurations at $\tilde{n} = 12$, which exponentially decays with the formula $\exp(-t/t_{\text{detach}})/t_{\text{detach}}$ as shown by the black line. In Fig. S5(b), we verify that the TF does a 1D random walk along the DNA. ΔX_c is the displacement of the center of mass along the DNA direction. $\langle \Delta X_c^2 \rangle \tilde{n}$ collapses, which means that c is nearly a constant independent of \tilde{n} . c is around 0.5, indicating the 1D diffusion coefficient is 50% of the 3D diffusion coefficient, shown in the inset of Fig. S5(b). It implies that the 1D “octopusing” walk is swift when the binding energy is small. (Note that c is at most equal to 1.) At large $\tilde{n} = 20$, the TF walks for ~ 100 bp along the DNA before detaching. This distance is comparable to the optimal length L^* observed for the optimal search with relatively small \tilde{n} and large E_B . Although its 1D search time is shorter than that of the optimal search, most of the search time is spent on 3D search due to a large \tilde{n} . As a result, the total search time here is longer than the optimal search time.

We also find that the Transition Probability Matrix W of the number of bound sites n can describe the detailed

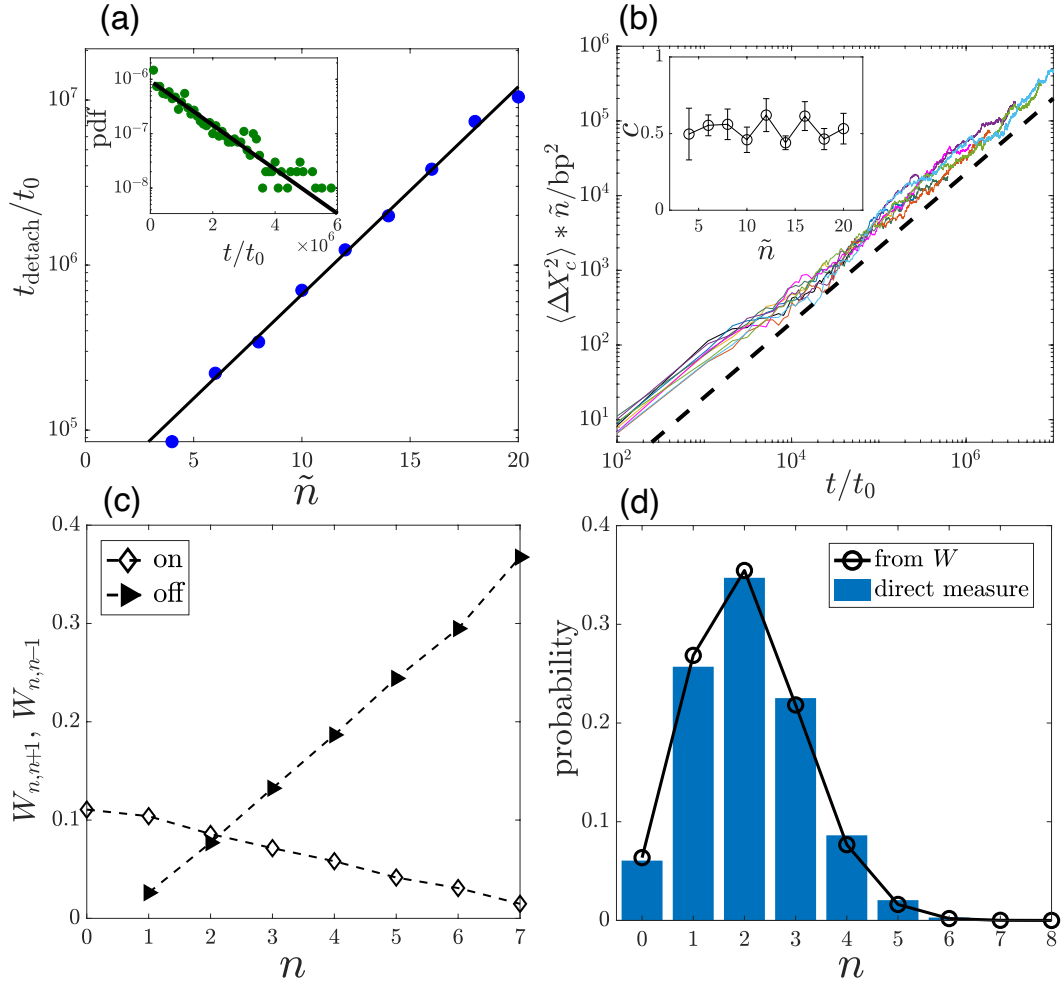


Figure S5. (a) t_{detach} vs. \tilde{n} . The black line is a guide for the exponential increase. Inset: Probability distribution of individual off-time at $\tilde{n}=12$, which satisfies $\exp(-t/t_{\text{detach}})/t_{\text{detach}}$. (b) Collapse $\langle \Delta X_c^2 \rangle \tilde{n}$ vs. t . The black dashed line, linear in t , is added as a guide. Inset shows c extracted from $\langle \Delta X_c^2 \rangle$ varying with \tilde{n} . (c) $W_{n,n+1}$ (or $W_{n,n-1}$) denoted by “off” (or “on”) varies with n . (d) Probability distribution of bound sites.

balance of the TF walking along DNA. The probability $P(n, t)$ satisfies $P(n, t+dt) = P(n, t)W$. At small dt , W is a tridiagonal matrix. Fig. S5(c) shows $W_{n,n+1}$ (or $W_{n,n-1}$) varying with n at small $dt = 0.1t_0$. We find that both are approximately linear with \tilde{n} , which implies that the off-rate and on-rate for each site are constants. There exists a maximal probability at $n \approx 2$ corresponding to $W_{n,n+1} = W_{n,n-1}$, suggesting that the “octopus” walk along DNA with two sites in the bound state has the highest probability. In the steady state, $P(n, t \rightarrow \infty)$ approaches the eigenstate of W with the largest eigenvalue (≈ 1). $P(n, t \rightarrow \infty)$ calculated from W is shown with the black dotted line in Fig. S5(d). It is consistent with the direct measure of the probability displayed by the bars in Fig. S5(d). It verifies that the TF walking along DNA is in a dynamic steady state.

S7. Advantage of the single round of 3D-1D search

In this section, we show that our minimal search time t_{min} in a single round of 3D-1D search process is significantly shorter compared to the minimal search time obtained when multiple rounds of 3D-1D excursions take place, as in the facilitated diffusion (FD) model. We note an important difference between the FD model and the one we propose here: In the FD model, binding is assumed to occur throughout the entire genome, hence L is fixed to be the genome

length. In contrast, within our model the region of binding is assumed to be a free variable, as well as the binding energy E_B . Consider our model in the regime where E_B is small, and hence the rate of TF detachment from DNA (denoted as Γ) is high. In this scenario, analogously to the FD model, multiple rounds of 3D-1D excursions become necessary to find the target. In this regime, the 1D mean diffusion distance L_s , defined as $L_s = 2\sqrt{D_1\Gamma^{-1}}$ [30], is significantly smaller than L . As a result, the 1D total search time is proportional to L rather than L^2 [14, 15, 30, 31]. In the FD model [32] and based on our numerical observation (see Fig. S4 (a)), increasing E_B leads to a decrease in both D_1 and Γ , but an increase in L_s . Thus, we assume that L_s increases with E_B . The total search time can be calculated as $\frac{L}{L_s} (\tilde{t}_{3D} + \Gamma^{-1})$, where \tilde{t}_{3D} represents one round of 3D search time. By optimizing E_B , the minimal search time t_{FD} is achieved at \tilde{E}_B , where $\tilde{t}_{3D} = \Gamma^{-1}(\tilde{E}_B) \left(2\left(\frac{d\ln D_1}{d\ln \Gamma^{-1}} + 1\right)^{-1}\Big|_{E_B=\tilde{E}_B} - 1\right)$. Since $d\ln D_1/d\ln \Gamma^{-1}$ slowly varies with E_B , \tilde{t}_{3D} decreases with decreasing \tilde{E}_B . Since $d\ln D_1/d\ln \Gamma^{-1}$ is negative, $\tilde{t}_{3D} > \Gamma^{-1}(\tilde{E}_B)$. Therefore, the the minimal search time is given by $t_{FD} \sim \frac{L}{L_s(\tilde{E}_B)} \tilde{t}_{3D}$. (If D_1 is independent of E_B , $\tilde{t}_{3D} = \Gamma^{-1}(\tilde{E}_B)$ and $t_{FD} = \frac{2L}{L_s} \tilde{t}_{3D}$.)

We can show that t_{FD} is an increasing function of L .

- For the factor $L_s(\tilde{E}_B)$: as L increases, \tilde{t}_{3D} decreases and subsequently \tilde{E}_B decreases. Consequently, $L_s(\tilde{E}_B)$ also decreases.
- For the factor $L * \tilde{t}_{3D}$: at $L \leq R$ where R is the nucleus size, since $\tilde{t}_{3D} = t_{3D} \propto \ln(L)/L$ (see Eq. (6) in the main text), $L * \tilde{t}_{3D} \propto \ln L$. At $L > R$, since \tilde{t}_{3D} decreases at a slower rate than $\ln(L)/L$, $L * \tilde{t}_{3D}$ increases more rapidly than $\ln L$. Thus, $L * \tilde{t}_{3D}$ is an increasing function of L .

Therefore, t_{FD} increases with L . We only need to consider a L where $L < L^*$. Clearly,

$$t_{FD} \sim \frac{L}{L_s} \tilde{t}_{3D}(L) \gg \tilde{t}_{3D}(L) = t_{3D}(L) > t_{3D}(L^*) \sim t_{\min}. \quad (\text{S11})$$

The significantly short t_{\min} emphasizes the advantage of our search mechanism. In reality, as we decrease L , since \tilde{E}_B increases, the corresponding L_s increases, causing the ratio L_s/L to approach 1. Thus, a single round of search instead of multiple rounds becomes the optimal search.